Research Article
Molecular and Cell Biology

JOURNAL
OF HEPATOLOGY

Generation of expandable human pluripotent stem cell-derived hepatocyte-like liver organoids

Graphical abstract

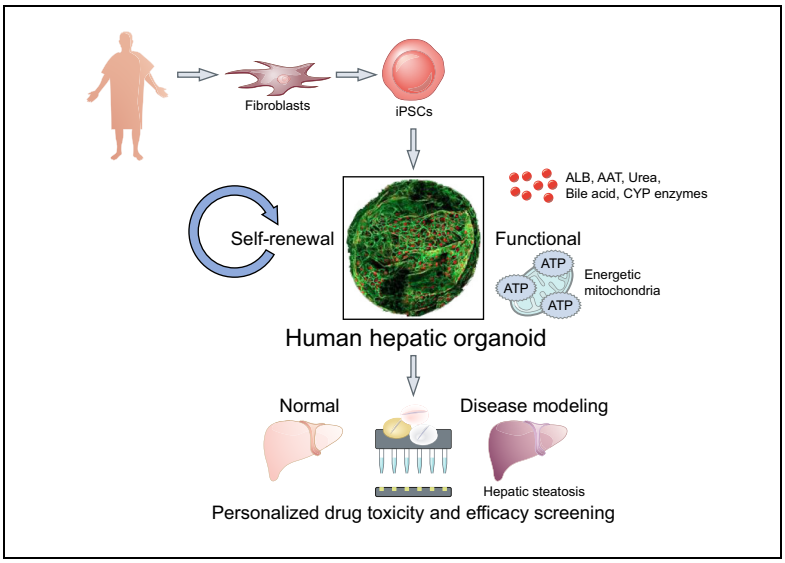

Highlights

- Pluripotent stem cell (PSC)-derived expandable human hepatocyte-like liver organoids were generated.
- PSC-derived human hepatic organoids are capable of long-term expansion with competent liver functionality.
- PSC-derived human hepatic organoids provide a robust hepatic model for toxicity prediction and drug screening.

Authors

Seon Ju Mun, Jae-Sung Ryu, Mi-Ok Lee, ..., Cho-Rok Jung, Kyung-Sook Chung, Myung Jin Son

Correspondence

kschung@kribb.re.kr
(K.-S. Chung) mjson@kribb.re.kr
(M.J. Son)

Lay summary

A functionally mature, human cell-based liver model exhibiting human responses in toxicity prediction and drug evaluation is urgently needed for pre-clinical drug development. Here, we develop a novel human pluripotent stem cell-derived hepatocyte-like liver organoid that is critically advanced in terms of its generation method, functional performance, and application technologies. Our organoids can contribute to the better understanding of liver development and regeneration, and provide insights for metabolic studies and disease modeling, as well as toxicity assessments and drug screening for personalized medicine.

http://dx.doi.org/10.1016/j.jhep.2019.06.030
 J. Hepatol. 2019, 71, 970–985

Research Article
Molecular and Cell Biology

JOURNAL OF HEPATOLOGY

Generation of expandable human pluripotent stem cell-derived hepatocyte-like liver organoids

Seon Ju Mun[1,2], Jae-Sung Ryu[1], Mi-Ok Lee[1], Ye Seul Son[1,2], Soo Jin Oh[3], Hyun-Soo Cho[1,2], Mi-Young Son[1,2], Dae-Soo Kim[2,4], Su Jung Kim[3], Hyun Ju Yoo[3], Ho-Joon Lee[1], Janghwan Kim[1,2], Cho-Rok Jung[1,2], Kyung-Sook Chung[1,2,5,*], Myung Jin Son[1,2,*]

[1]*Stem Cell Convergence Research Center, Korea Research Institute of Bioscience and Biotechnology (KRIBB), 125 Gwahak-ro, Yuseong-gu, Daejeon 34141, Republic of Korea;* [2]*Department of Functional Genomics, Korea University of Science & Technology (UST), 217 Gajungro, Yuseong-gu, Daejeon 34113, Republic of Korea;* [3]*Convergence Medicine Research Center, Asan Institute for Life Sciences, Asan Medical Center, University of Ulsan College of Medicine, Seoul 05505, Republic of Korea;* [4]*Environmental Diseases Research Center, KRIBB, 125 Gwahak-ro, Yuseong-gu, Daejeon 34141, Republic of Korea;* [5]*Biomedical Translational Research Center, KRIBB, 125 Gwahak-ro, Yuseong-gu, Daejeon 34141, Republic of Korea*

Background & Aims: The development of hepatic models capable of long-term expansion with competent liver functionality is technically challenging in a personalized setting. Stem cell-based organoid technologies can provide an alternative source of patient-derived primary hepatocytes. However, self-renewing and functionally competent human pluripotent stem cell (PSC)-derived hepatic organoids have not been developed.

Methods: We developed a novel method to efficiently and reproducibly generate functionally mature human hepatic organoids derived from PSCs, including human embryonic stem cells and induced PSCs. The maturity of the organoids was validated by a detailed transcriptome analysis and functional performance assays. The organoids were applied to screening platforms for the prediction of toxicity and the evaluation of drugs that target hepatic steatosis through real-time monitoring of cellular bioenergetics and high-content analyses.

Results: Our organoids were morphologically indistinguishable from adult liver tissue-derived epithelial organoids and exhibited self-renewal. With further maturation, their molecular features approximated those of liver tissue, although these features were lacking in 2D differentiated hepatocytes. Our organoids preserved mature liver properties, including serum protein production, drug metabolism and detoxifying functions, active mitochondrial bioenergetics, and regenerative and inflammatory responses. The organoids exhibited significant toxic responses to clinically relevant concentrations of drugs that had been withdrawn from the market due to hepatotoxicity and recapitulated human disease phenotypes such as hepatic steatosis.

Conclusions: Our organoids exhibit self-renewal (expandable and further able to differentiate) while maintaining their mature hepatic characteristics over long-term culture. These organoids may provide a versatile and valuable platform for physiologically and pathologically relevant hepatic models in the context of personalized medicine.

Lay summary: A functionally mature, human cell-based liver model exhibiting human responses in toxicity prediction and drug evaluation is urgently needed for pre-clinical drug development. Here, we develop a novel human pluripotent stem cell-derived hepatocyte-like liver organoid that is critically advanced in terms of its generation method, functional performance, and application technologies. Our organoids can contribute to the better understanding of liver development and regeneration, and provide insights for metabolic studies and disease modeling, as well as toxicity assessments and drug screening for personalized medicine.

Introduction

Human cell-based and personalized *in vitro* liver models are urgently needed for drug efficacy and toxicity tests in preclinical drug development. Although the liver is a representative organ with a native regenerative potential *in vivo*, primary human hepatocytes (PHHs), which are considered the gold standard for evaluating hepatic metabolism, are limited by their loss of proliferative capacity and long-term functionality *in vitro*.[1] To overcome the limitations of PHHs, various approaches have been developed, including genetic modification,[2] 3D culture combined with tissue engineering technologies,[1,3–7] and defined medium compositions.[8,9] However, the development of alternative and sustainable cell sources to recapitulate the function of native liver remains challenging.

Stem cells are a useful alternative source of liver cells, which can be obtained from various methods, including the differentiation of hepatic cells from pluripotent stem cells (PSCs),[10–15] direct conversion,[16–19] and from tissue stem cells.[20–23] Importantly, compared with conventional 2D cultures, 3D configurations, such as spheroids or organoids confer advantages for the differentiation ability of stem cells and the maintenance of metabolic function.[5] Liver bud generation from PSCs[24–28] and

Keywords: Liver; Organoids; Pluripotent stem cells; Drug toxicity; Disease modeling; Hepatocytes.
Received 19 October 2018; received in revised form 19 June 2019; accepted 21 June 2019; available online 9 July 2019

* Corresponding authors. Address: Stem Cell Convergence Research Center, Korea Research Institute of Bioscience and Biotechnology (KRIBB), 125 Gwahak-ro, Yuseong-gu, Daejeon 34141, Republic of Korea. Son MJ; Tel.: +82 42 860 4477; Fax: +82 42 860 4608. Chung K; Tel.: +82 42 860 4179, Fax: +82 42 860 4597.
E-mail addresses: kschung@kribb.re.kr (K.-S. Chung), mjson@kribb.re.kr (M.J. Son).

liver organoid generation from primary liver tissues[21,22] are leading-edge technologies in the development of stem cell-based *in vitro* 3D liver models. However, as its name implies, liver buds from PSCs present fetal characteristics *in vitro* before transplantation, and most importantly, it is not a proliferative system. Tissue-derived hepatic organoids have limitations in accessibility to human tissue and a narrow differentiation potential, although these organoids are expandable and maintain mature functionality. Therefore, we have adapted both technologies to allow for the generation of proliferative and more mature hepatic organoids derived from PSCs, including human embryonic stem cells (hESCs) and induced pluripotent stem cells (iPSCs), which are a renewable source of parenchymal and non-parenchymal tissue cells. In genomic and functional analyses, our hepatocyte-like liver organoids manifested more mature phenotypes compared with those of 2D differentiated hepatocytes and tissue-derived hepatic organoids. Notably, our system reproducibly provides a robust hepatic model for toxicity prediction, regenerative and inflammatory responses, modeling for diseases such as hepatic steatosis, and drug screening.

Materials and methods

Hepatocyte differentiation/organoid generation

Hepatic differentiation was performed by using previously described protocols with modifications.[10,25,26] For definitive endoderm differentiation, PSCs were cultured on Matrigel-coated dishes under PSC medium for 3 days, and then the medium was exchanged with RPMI 1640 (Thermo Fisher; 11875-093) supplemented with 1xB-27™ without insulin (Thermo Fisher; A1895601) and 100 ng/ml human activin A (PeproTech; 120-14e) and incubated for 6 days. For hepatic endoderm differentiation, the medium was exchanged with RPMI 1640 supplemented with 1xB-27 (Thermo Fisher; 17504-044), 10 ng/ml bFGF, and 20 ng/ml human BMP-4 (PeproTech; 120-05ET) for 4 days under 5% hypoxia conditions. For hepatic maturation, the medium was exchanged with Hepatocyte Culture Medium (Lonza; CC-3198) without EGF, diluted with Endothelial Cell Growth Medium-2 (Lonza; CC-3162) (1:1) supplemented with 2.5% FBS, 100 nM dexamethasone (Sigma-Aldrich; D4902), 20 ng/ml OSM (R&D system; 295-OM-050), and 10 ng/ml of HGF (PeproTech; 100-39) for 4 days under hypoxia and then an additional 8 days of culture under normoxia. Approximately 9 to 12 days after hepatic maturation, 3D spherical structures appeared over 2D monolayers of mature hepatocytes. The floating cysts were collected and solidified with Matrigel as a dome, and then hepatic medium (HM) was added. The medium compositions are shown in Table S1.

Organoid culture

Organoids were routinely maintained in HM, and the medium was replaced every 3 days. The organoids were mechanically passaged every 7 days; they were washed with cold PBS to remove the Matrigel and split into small pieces by a surgical blade under a dissecting microscope. The passaged organoids were then resuspended in Matrigel at a 1:3–1:10 ratio. Alternatively, organoids were chemically passaged with Gentle Cell Dissociation Reagent (Stem Cell Technology; ST07174) by pipetting approximately 15 times. For cryopreservation, the passaged organoids were mixed with mFreSR™ (Stem Cell Technology; 05855), and freezing/thawing was performed by standard procedures. After thawing, 10 μM Y-27632 (Tocris; 1254) was added to the medium for 3 days. Tissue-derived organoids were generated from IRB-approved human adult liver tissue according to a previously described protocol.[21] For further differentiation of hepatic organoids, HM-cultured organoids were incubated under expansion medium (EM) supplemented with 20 ng/ml BMP7 (PeproTech; 120-03) for 2–3 days and then under differentiation medium (DM) for an additional 6 days. The medium compositions are shown in Table S1.

Functional studies

To analyze glycogen storage, organoids were fixed with 4% paraformaldehyde (Biosesang; P2031), cryo-protected in 30% sucrose, and frozen in optimal-cutting-temperature compound (Sakura Finetek; 4583). Frozen sections were sliced to a thickness of 10 μm at −20 °C with a cryostat microtome (Leica). Sectioned samples were stained with periodic acid-Schiff (IHC World; IW-3009) according to the manufacturer's instructions. For indocyanine green (ICG) uptake and release, organoids were washed with cold PBS to remove the Matrigel and incubated with 1 mg/ml of ICG (Sigma; I2633) for 15 min at 37 °C in 5% CO_2. Images of ICG uptake were taken under a microscope, then the organoids were gently washed 3 times with PBS, and fresh medium was added. After 1 h of incubation at 37 °C in 5% CO_2, images of ICG release were taken under a microscope. For albumin (ALB), α1-antitrypsin (AAT), and urea quantitation, medium was collected at 48 h after the medium change and analyzed using a Human Albumin ELISA Kit (Bethyl Laboratories; E80-129), Human Alpha-1-Antitrypsin ELISA Quantitation Kit (GenWaybio; GWB-1F2730), or Urea Assay Kit (Cell Biolabs, Inc.; STA-382) following the manufacturer's instructions. The absorbance was detected by a Spectra Max M3 microplate reader (Molecular Devices), and the data were normalized by the cell number. For CYP activity, CYP enzymes were induced by treatment with each inducer (CYP3A4; 20 μM rifampicin, 100 μM acetaminophen, and 10 μM nifedipine and CYP1A2; 150 μM omeprazole) for 48 h. CYP enzyme activities were measured after 3 h of incubation with each subtype-specific substrate using a P450-Glo Assay Kit (Promega; V9002 for 3A4 and V8422 for 1A2). Luciferase activity was then measured using a luminometer (Victor X Light, Perkin Elmer) and the data were normalized by the cell number. For the functional polarization assay, organoids were removed from the Matrigel and incubated with culture media supplemented with 10 μg/ml CDFDA (Sigma; 21884) and 1 μg/ml Hoechst 33342 (Invitrogen; 62249) for 30 min at 37 °C in 5% CO_2. The organoids were gently washed twice with cold PBS containing calcium and magnesium. Culture medium was added and then fluorescence images were obtained under a confocal microscope at 37 °C in 5% CO_2. For bile acid quantification, the organoids were lysed by homogenization with PBS and then analyzed using a Total Bile Acid Assay Kit (Biovision; K209-100). The observance was measured by a Spectra Max M3 microplate reader, and the data were normalized by the cell number.

Statistical analysis

All figures show representative data of more than 3 independent biological replicates. The graphs represent the mean ± SEM. Quintuplicate samples were used for the oxygen consumption rate (OCR) analysis; triplicate samples were used for the PCR analysis, ELISA, metabolite analysis, toxicity test, Nile red and Oil red O staining, and CYP activity (technical replicates).

Student's *t* test was used to evaluate the inter-group comparisons, and $p < 0.05$ indicated statistical significance. All analyses of statistical significance were performed by comparison with the control group unless otherwise indicated.

Results

Generation of expandable human hepatic organoids from PSCs

To obtain mature hepatocytes from PSCs, we applied conventional 2D differentiation protocols based on the liver developmental process described by the Duncan[10] and Taniguchi[25] groups with slight modifications (Fig. 1A). In brief, fully characterized and integration-free human iPSCs (Fig. S1A-D) or hESCs were differentiated in a stepwise fashion into definitive endoderm (DE)-, hepatic endoderm (HE)-differentiated cells, immature hepatocytes (IH), and mature hepatocytes (MH) (Fig. S1E). The DE differentiation process, which is an initial and important intermediate stage of hepatic development during organogenesis, was optimized (Fig. S2A) by treatment with B27 without insulin and Activin A[29] based on the mRNA (Fig. S2B) and protein (Fig. S2C) expression of DE markers, such as SOX17 and FOXA2. The expression of each stage-specific marker during differentiation was examined at both the mRNA (Fig. S3A) and protein (Fig. S3B) levels. Approximately 22 days after starting differentiation, 3D spherical structures appeared over 2D monolayers of MHs (Fig. 1B) and a cuboidal cell morphology similar to that of parenchymal liver cells was clearly recognized on the surface of the globular structure (Fig. 1C). This 3D structure was comparable to that of tissue-derived liver organoids comprising a single-layered epithelium;[22,30] therefore, we adapted culture systems for human liver organoids from Clevers' group.[22] However, to simultaneously intensify the self-renewal potential and hepatic characteristics of organoids, we modified the media composition of the EM by additional treatment with basic fibroblast growth factor (bFGF), oncostatin M (OSM), insulin-transferrin-selenium (ITS), and dexamethasone, except for R-spondin and fibroblast growth factor 10 (FGF 10), and designated it HM (Table S1). In the Matrigel-embedded HM culture condition, 3D organoids were significantly enlarged during 5 days of culture (Fig. S4A), could be passaged either by mechanical or enzymatic splitting (Fig. S4B), and regrew well even after freezing and thawing (Fig. S4C). The organoids were capable of self-renewal both in suspension and in Matrigel (Fig. 1D and Video S1) and expanded well for long-term culture (Fig. 1E). The organoids could be passaged more than 24 times over 5 months (Fig. S4D), stably maintained a normal karyotype over 3 months after *in vitro* culture (Fig. S4E), and matched the short tandem repeat prolife of original fibroblasts (Fig. S4F). Remarkably, E-cadherin-stained epithelial cells exhibited a Ki67-positive proliferative state with strong expression of ALB (Fig. 1F).

Characterization of human hepatic organoids from PSCs

Next, the characteristics of established 3D organoids were compared among the iPSCs, HEs, and 2D differentiated mature hepatocytes (2D MHs) (Fig. 2). When the gene expression levels of stage-specific markers were compared with the 2D MHs, the organoids exhibited lower expression of the pluripotency marker *NANOG*, maintained the expression of the adult stem cell marker *LGR5*, and expressed similar or higher levels of the ductal markers *SOX9* and *CK19* and the MH markers *ALB*, *TTR*, *CK18*, and *RBP4* (Fig. 2A). High expression levels of epithelial markers (E-cadherin and ZO1), hepatocyte markers (HNF4A, ALB, AAT, and PEPCK), a bile salt efflux transporter (MRP4), ductal markers (CK19 and SOX9), and an adult stem cell marker (LGR5) were observed in the HM-cultured organoids by immunofluorescence (Fig. 2B). A detailed metabolism study associated with glucose, amino acid, and lipid metabolism was performed during organoid generation, and the distinct metabolic features among iPSCs, HEs, 2D MHs, and organoids are explained in Figs. S5 and S6. Highly proliferating iPSCs represented dominant glycolytic activity, and the tricarboxylic acid cycle and oxidative phosphorylation (OXPHOS) pathways were increased upon

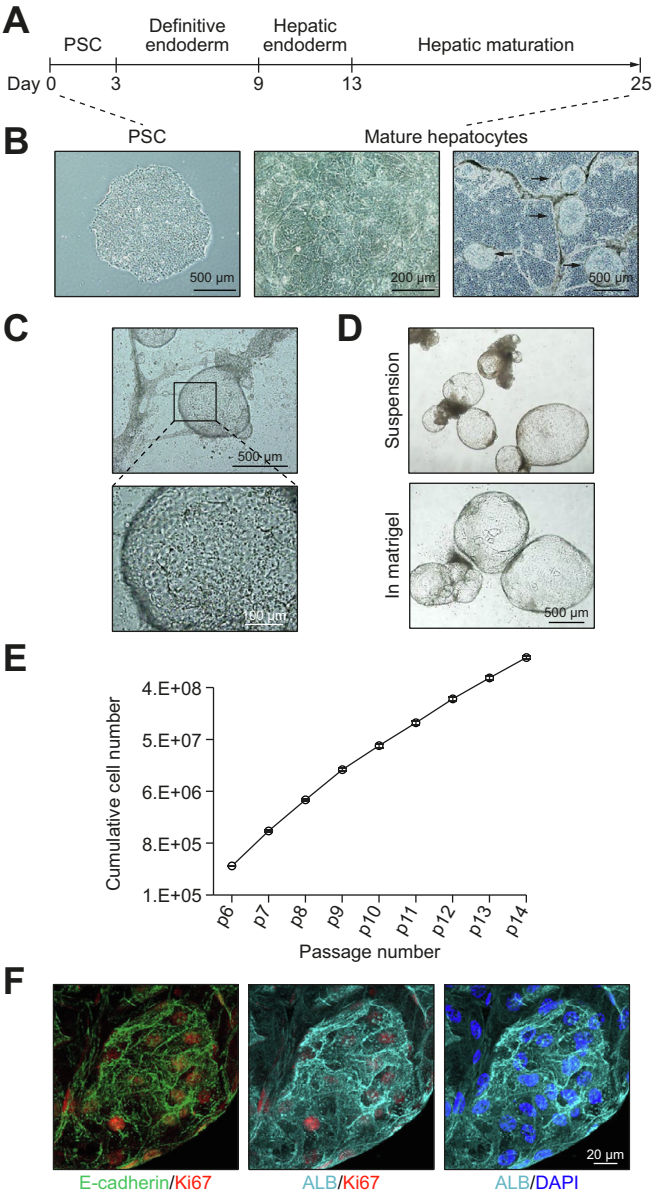

Fig. 1. Generation of expandable human hepatic organoids from PSCs. (A) Scheme of hepatic organoid generation. (B) Representative morphology of PSCs before starting differentiation (left), matured hepatocytes in the 2D monolayers (middle), and organoids (right). Arrows indicate floating 3D organoids over 2D cells. (C) Enlarged image of the organoid in the upper panel (black square) is shown in the lower panel. (D) Representative morphology of organoids in suspension culture and in Matrigel. (E) Graph presents calculated cumulative cell number at each passage of the organoids. Data are the mean ± SEM (n = 3). (F) Representative immunofluorescence images of organoids stained with each indicated antibody. PSCs, pluripotent stem cells.

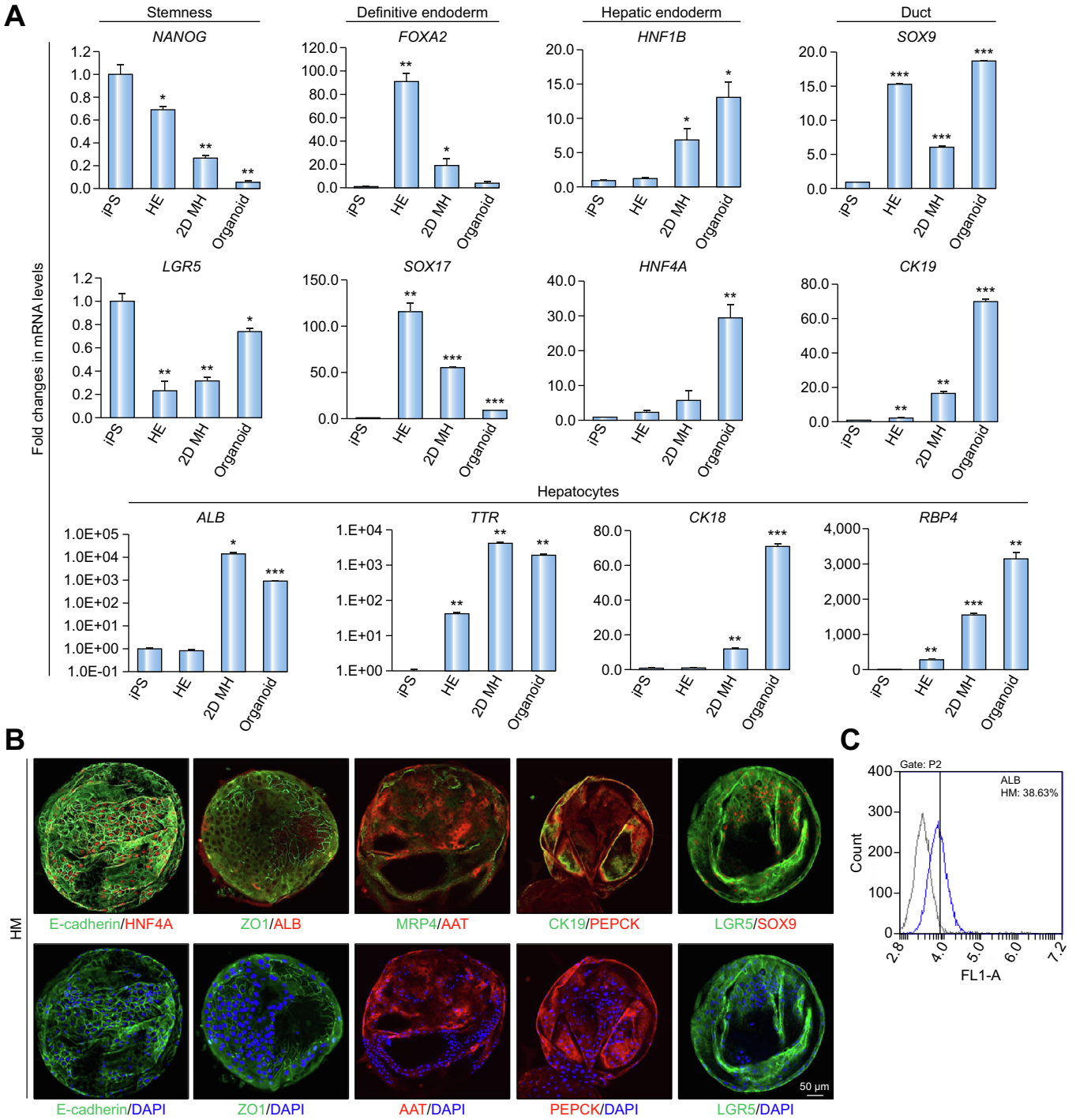

Fig. 2. Characterization of human hepatic organoids from PSCs. (A) mRNA expression levels of each specific marker in the iPSCs, HEs, 2D MHs, and organoids. Data are the mean ± SEM (n = 3) and analyzed by Student's *t* test, $^{*}p$ <0.05; $^{**}p$ <0.01; and $^{***}p$ <0.001. (B) Representative immunofluorescence images of organoids stained with each indicated antibody. (C) Representative FACS analysis of organoids stained with ALB. 2D MHs, 2D differentiated mature hepatocytes; HEs; hepatic endoderm-differentiated cells; iPSC, induced pluripotent stem cells.

differentiation in a liquid chromatography-mass spectrometry (LC-MS)-based metabolite analysis (Fig. S5) and whole-genome transcriptome analysis (Fig. S6). We also established 2 hESC line-derived organoids from H1 and H9 cells and 2 in-house iPSC line-derived organoids from human foreskin fibroblasts (iPS_1) and human liver fibroblasts (iPS_2) (Fig. S7). The organoids were reproducibly generated without interline variability in the organoid generation efficiency, morphological characteristics (Fig. S7A), self-renewal capacity, and marker expression (Fig. S7B). Representatively, the ALB^{+} mature hepatocyte population was quantified in the iPS_1-derived organoids, which accounted for 38.63% in the FACS analysis (Fig. 2C).

Differentiation of human hepatic organoids towards mature characteristics

Organoids were found to be more differentiated under defined culture conditions, which involved culturing with EM and subsequently with DM[22] (Table S1). As Huch *et al.* reported, the addition of BMP7 with EM before the DM treatment was the most effective condition for increasing the expression of *ALB* and *CYP3A4* (Fig. S8A and B, condition e). We then optimized the time course of differentiation based on ALB secretion (Fig. S8C and D), which allowed us to finally refine the differentiation condition presented in Fig. 3A (Fig. S8C and D, condition i). Under any condition, the organoids secreted much more ALB compared with a 3D culture of differentiated HepaRG cells, a widely used liver progenitor cell line[31,32] (Fig. S8D). EM-cultured organoids presented an enlarged spherical structure, and DM-cultured organoids had a smaller and packed morphology compared with that of HM-cultured organoids (Fig. 3B). The differentiated organoids (DM) expressed sufficient levels of mature hepatocyte makers, such as *ALB*, *TTR*, and cytochrome p450-3A4 (*CYP3A4*) and ductal marker *CK19*, compared with PHHs and human liver tissue (Fig. 3C). High expression levels of E-cadherin, HNF4A, ZO1, and PEPCK were maintained in both EM- and DM-cultured organoids (Fig. 3D). The expression of the mature hepatocyte markers ALB, AAT, and MRP2 (bile transporter) was strongly enhanced in DM, whereas the expression of CK19, LGR5, and SOX9 was decreased in DM compared with that in EM (Fig. 3D). The gene expression levels of *LGR5* and *SOX9* also showed greater decreases in the DM condition than the EM (Fig. S8E). Quantitatively, the ALB^{+} mature hepatocyte population occupied 53.85% of EM and 79.44% of DM in the FACS analysis (Fig. 3E). Upon differentiation, the organoids revealed more functionally mature hepatic cell characteristics (Fig. 4). Accumulated glycogen was strongly detected in differentiated organoids by periodic acid-Schiff staining (Fig. 4A) and ICG uptake and release, which was used as a functional assessment for human liver transplantation,[33] was functional for 15 min of incubation (Fig. 4B and Fig. S9A). However, undifferentiated iPSCs did not uptake ICG at all, even 1 h after incubation (Fig. S9B). The secretion of ALB was potently increased in differentiated organoids compared with that under either the 2D MH or HM conditions (Fig. 4C), which is consistent with the level of PHHs. The secretion of AAT was significantly higher in both the HM- and DM-cultured organoids than in the 2D MHs or PHHs (Fig. 4D). The levels were 6- to 8-fold higher than those

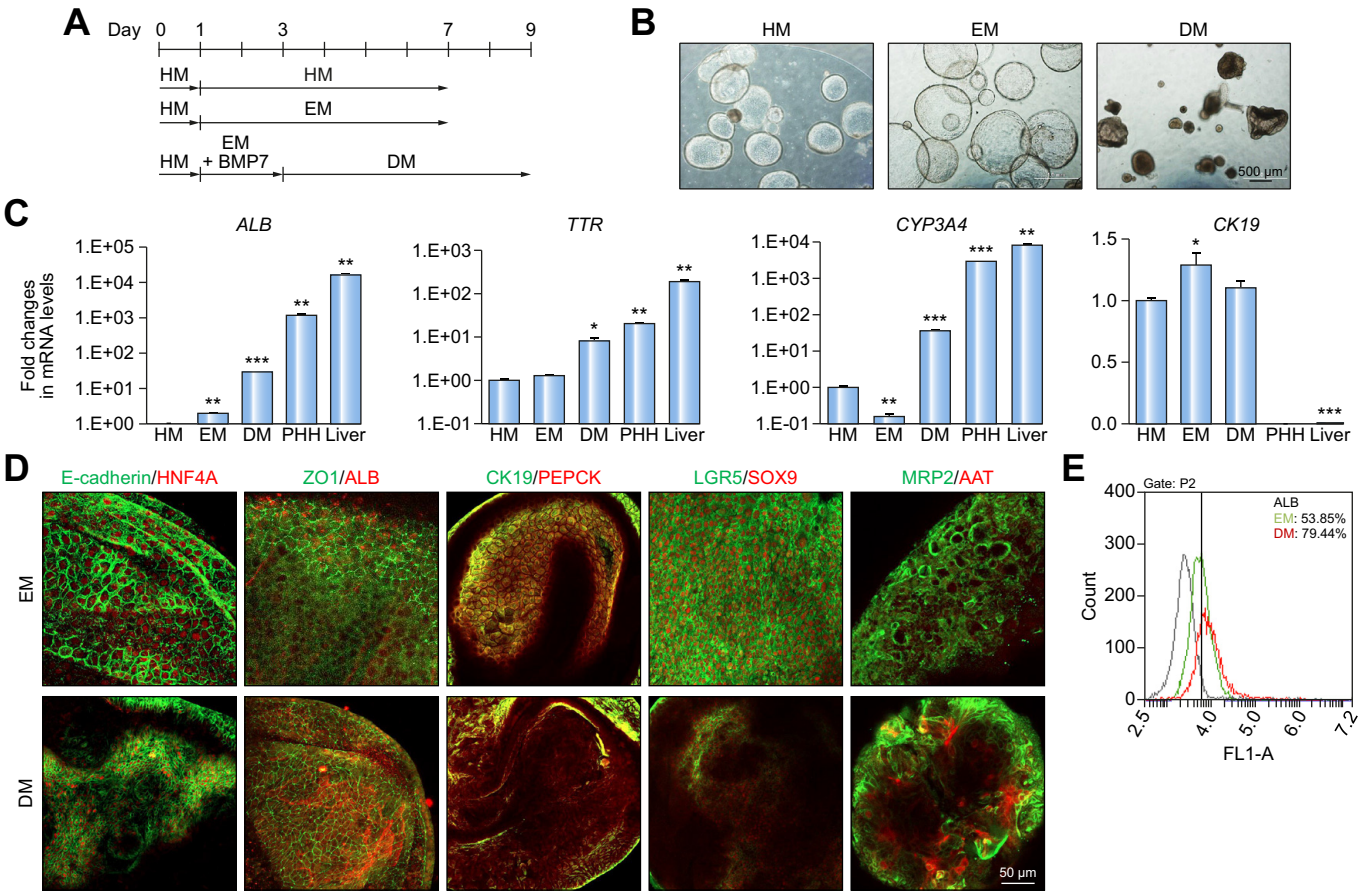

Fig. 3. Differentiation of human hepatic organoids. (A) Schematic diagram of the further differentiation of organoids. Continued HM-cultured condition was designated as " HM", the condition that HM-cultured organoids were incubated with EM for 6 days was designated as "EM", and the condition that HM-cultured organoids were incubated with EM with BMP7 for 2 days and then cultured with DM for 6 days designated as "DM". (B) Representative morphology of organoids in the HM, EM, and DM condition. (C) mRNA expression levels of each specific marker in the HM-, EM-, and DM-cultured organoids; PHHs; and human liver tissue. Data are the mean ± SEM (n = 3) and analyzed by Student's *t* test, $^{*}p$ <0.05; $^{**}p$ <0.01; and $^{***}p$ <0.001. (D) Representative immunofluorescence images of EM-cultured (upper panel) and DM-cultured (lower panel) organoids stained with each indicated antibody. (E) Representative FACS analysis of ALB in EM- and DM-cultured organoids. DM, differentiation medium; EM, expansion medium; HM, hepatic medium; PHHs, primary human hepatocytes.

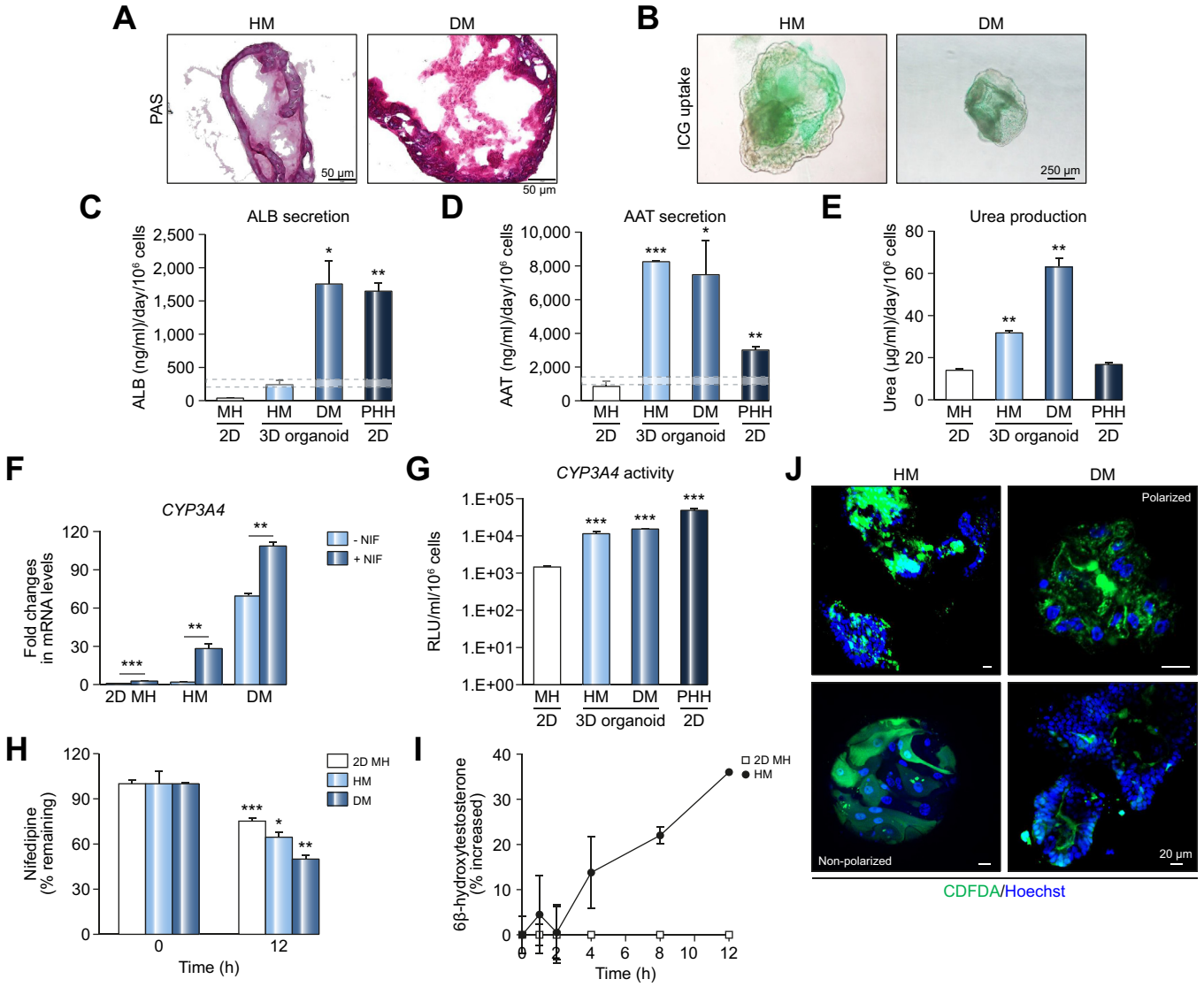

Fig. 4. Mature characteristics of the differentiated human hepatic organoids. (A) Representative images of HM- and DM-cultured organoids stained with PAS. (B) Representative images of HM- and DM-cultured organoids incubated with ICG for 15 min. Quantitation of (C) ALB, (D) AAT, and (E) urea production in the 2D MHs and HM- and DM-cultured organoids, and PHHs. Data are the mean ± SEM (n = 3) and analyzed by Student's *t* test. The levels from human liver tissue-derived organoids reported by Clevers[22] are indicated as dotted lines. (F) mRNA expression of *CYP3A4* in the 2D MHs and HM- and DM-cultured organoids with or without 10 μM NIF induction for 48 h. Data are the mean ± SEM (n = 3) and analyzed by Student's *t* test. (G) NIF-induced CYP3A4 enzyme activity in the 2D differentiated MH and HM- and DM-cultured organoids, and PHH. Data are the mean ± SEM (n = 3) and analyzed by Student's *t* test. (H) Relative level of residual NIF metabolized by 2D differentiated MHs and HM- and DM-cultured organoids after 12 h of treatment. Data are the mean ± SEM (n = 3) and analyzed by Student's *t* test. (I) Relative level of metabolized testosterone, 6β-hydroxytestosterone, in the 2D differentiated MHs and HM-cultured organoids over 12 h. Data are the mean ± SEM (n = 3) and analyzed by Student's *t* test. (J) Representative fluorescence images of bile canaliculi-like structures stained with CDFDA in the HM- and DM-cultured organoids. $^{*}p$ <0.05; $^{**}p$ <0.01; and $^{***}p$ <0.001. 2D MHs, 2D differentiated mature hepatocytes; DM, differentiation medium; HM, hepatic medium; ICG, indocyanine green; NIF, nifedipine; PAS, periodic acid-Schiff; PHHs, primary human hepatocytes; RLUs, relative luminescence units.

from human liver tissue-derived organoids as reported by Clevers' group.[22] Urea production was also increased in differentiated organoids (Fig. 4E). Notably, the gene expression levels of essential CYP families, which are important in drug metabolism and toxicity and include *CYP3A4*, *1A2*, *2A6*, and *2E1*, were enhanced in the HM-cultured organoids compared with the levels in the 2D MHs (Fig. S10A). Interestingly, the expression of *CYP3A7*, which is a fetal counterpart of *CYP3A4*[34] occupying a major proportion of CYP-mediated drug metabolism, was distinctly decreased in the organoids compared with the expression in the 2D MHs (Fig. S10A), suggesting the promotion of hepatic maturation in the organoids. The basal CYP3A4 activity of organoids was incomparable with that of the 2D HepG2 cells, which was strongly induced by treatment with rifampicin, acetaminophen (APAP), and nifedipine (Fig. S10B). Thus, we used nifedipine to induce CYP3A4 for further drug metabolism studies. The expression of *CYP3A4* was enriched in the DM-cultured organoids compared with that in the 2D MHs and HM-cultured organoids and was potently increased by nifedipine induction (Fig. 4F). Higher CYP3A4 activity was observed in both nifedipine-induced HM- and DM-cultured organoids, although it did not reach the level of PHH activity (Fig. 4G). The functional activity of CYP3A4 determined by the drug clearance potential of the remaining nifedipine in the supernatants was reduced

in the organoids compared with that in the 2D MHs (Fig. 4H), indicating the increased detoxifying function of the organoids. Moreover, even HM-cultured organoids directly hydroxylated testosterone into 6β-hydroxytestosterone (Fig. 4I), revealing the CYP3A4-mediated functionally mature drug-metabolizing activity of the HM-cultured organoids. In addition, polarized epithelial cells with bile canaliculi-like structures were well recognized in differentiated organoids by CDFDA staining (Fig. 4J), which is known to be barely detectable in the 2D monolayer culture systems.[35] Polarized epithelial cells were detected in only 21% of the 2D MHs and 28% of the PHHs in 10 fields of each group we photographed (Fig. S10C). Overall, these data revealed that the human hepatic organoids differentiated in our system exhibit functionally mature hepatocyte-like characteristics.

Transcriptome profiles and functional assessment of human hepatic organoids

Next, to further validate the maturity potential of the organoids, we analyzed their molecular profiles. We previously developed a liver-specific gene expression panel (LiGEP) algorithm, which is an RNA-sequencing-based validation platform that quantitatively evaluates the differentiation status of hepatocyte models and presents the degree of liver similarity.[36] Although the 2D MHs revealed liver similarity scores of 31.18%, the organoids presented similarities of 41.94%, 45.16%, and up to 60.22% under HM-, EM-, and DM-culture conditions, respectively (Fig. 5A). The levels of expressed genes in each sample are presented in Fig. 5B, and the list is provided in Table S2. The whole-genome transcriptome analysis revealed 4 significant clusters in which genes were highly expressed in human liver tissue (cluster 1), in the organoids compared with iPSCs and 2D MHs (cluster 2), in DM-cultured organoids (cluster 3), and in iPSCs (cluster 4) (Fig. S11A). Cluster 1 contained complement component genes, such as *C3* and *C1S*, resulting from the lack of an immune system in an *in vitro* liver model. Cluster 2 genes enriched in the organoids similar to the liver, contained gene sets for drug metabolism including phase I and II enzymes, peroxisome, the FOXA2 and FOXA3 transcription factor network related to liver regeneration, lipid metabolism including retinoid and steroid metabolism (Fig. S11B), as well as well-known hepatocyte markers, such as *TTR*, *HNF1A*, *HNF4A*, and *SERPINA1 (AAT1)* (Fig. 5C). Cluster 3 contained hepatic progenitor markers such as *AFP*, *KRT19*, and *DLK1*, and reflected less differentiation characteristics of organoids than adult liver tissue (Fig. S11A). As expected, cluster 4 contained pluripotency markers such as *SOX2*, *POU5F1 (OCT4)*, and *LIN28A* (Fig. S11C). Gene sets related to cell division were enriched in the gene ontology map of cluster 4 (Fig. S11D), and mitotic DNA replication-related pathways were augmented in the iPSCs (Fig. S11E). Additional details from cluster 2 indicated that gene sets for lipid, cholesterol, and alcohol metabolic processes, organic substance catabolic processes, and cell secretion were enriched in the gene ontology map (Fig. 5D), while cholesterol biosynthesis and complement and coagulation cascades were the top 2 pathways augmented in the organoids (Fig. 5E). Furthermore, we analyzed enriched pathways in differentiated organoids compared with those of 2D MHs, and the pathways involved in OXPHOS, bile acid metabolism, fatty acid metabolism (Fig. 5F), xenobiotic metabolism, coagulation, and peroxisome (Fig. S11F) were the top-ranked subset signatures of DM-cultured organoids. The expression of representative genes in each pathway was confirmed by real-time PCR (Fig. S12A). Surprisingly, the OCR as a surrogate of mitochondrial OXPHOS activity was potently increased in the organoids compared with that in the 2D MHs normalized by cell numbers (Fig. 5G), while basal and maximal respiration and respiration capacity were all remarkably higher in the organoids than in the 2D MHs (Fig. 5H). These real-time monitoring bioenergetics profiles revealed that both mitochondria- and glycolysis-dependent ATP production rates were increased in the organoids compared with those in the 2D MHs (Fig. S12B), resulting in an elevated total ATP production rate in the organoids (Fig. S12C). More importantly, the OCR of HM- or DM-cultured organoids was similar to that of adult liver tissue-derived hepatic organoids (Fig. 5G and Fig. S13). Tissue-derived organoids were also well established (Fig. S13A) and differentiated (Fig. S13B), but the growth rate and differentiation response were slightly reduced and the level and rate of ALB production in the tissue-derived organoids were lower than those in our PSC-derived organoids (Fig. S13C). Next, the bile acid production level was also heightened in the differentiated organoids compared with that in the HepG2 cells or 2D MHs (Fig. 5I), suggesting functional competence of the PSC-derived organoids. Therefore, our system acted as a pertinent platform of a functionally mature liver model and allowed us to test applications of toxicity prediction, disease modeling, and drug screening. These applications were performed under the HM condition because HM-cultured organoids have enough matured hepatic functionality over long-term culture, and it is a timely and cost-effective condition for further applications because it does not need an additional maturation process with EM and DM.

Toxicological outcomes prediction using human hepatic organoids

In transcriptome profiles, organoids potently expressed phase I drug-metabolizing CYP enzymes and phase II detoxification enzymes at a level similar to that of liver tissue (Fig. 6A), which is rapidly lost[2] in the 2D cultured-hepatocyte models. The activities of CYP1A2 (Fig. 6B) were well induced by omeprazole treatment in the HM-cultured organoids as well as CYP3A4 (Fig. 4G), although it did not reach the level of PHH activity. Thus, we compared the toxicity profiles of CYP3A4- and CYP1A2/2E1-mediated hepatotoxic drugs (troglitazone and APAP, respectively) between the 2D MHs and HM-cultured organoids (Fig. S14). While the control compound was cytotoxic (rotenone) or safe (dexamethasone) in the 2D MHs and organoids, the toxicity responses against troglitazone and APAP were different between the 2D and 3D models (Fig. 6C and Fig. S14A-D). The toxic concentration (TC_{50}) based on cell viability clearly showed the toxic sensitivity of the organoids compared with that of the 2D MHs (Fig. 6D and Fig. S14E). The sensitivity was further confirmed by real-time monitoring of reactive oxygen species (ROS) generation, glutathione (GSH) content, and nuclei structure in a chronic exposure model (Fig. S15). Troglitazone, an antidiabetic drug, was withdrawn from the market due to serious idiosyncratic hepatotoxicity, and it presented cytotoxicity with the 2 μM treatment, which did not reach the level of that with the maximal human exposure concentration (Cmax = 6.29 μM), *i.e.* a clinically relevant dose[37] (Fig. S15A). Next, we compared the effects of 2 structurally related antibiotics: trovafloxacin, which was withdrawn from the market due to patient death from liver failure; and levofloxacin, which is the non-toxic analogue of trovafloxacin.[38,39] As expected, levofloxacin did not show cytotoxicity over the Cmax

(23.8 μM), regardless of the 2D or 3D model (Fig. S16A and C). However, trovafloxacin led to a significant decrease in the cell viability of the organoids (Fig. S16B), which was not identified in the 2D conventional pre-clinical models.[37] Interestingly, 0.8 μM and 4 μM trovafloxacin treatments potently reduced the cell numbers in the HM-cultured organoids, while there was little or no toxicity in the 2D MHs at these concentrations (Fig. 6E). The non-toxic analogue, levofloxacin, only presented toxicity at the highest concentration tested (100 μM), which produced a 36% decrease in the cell viability of the organoids

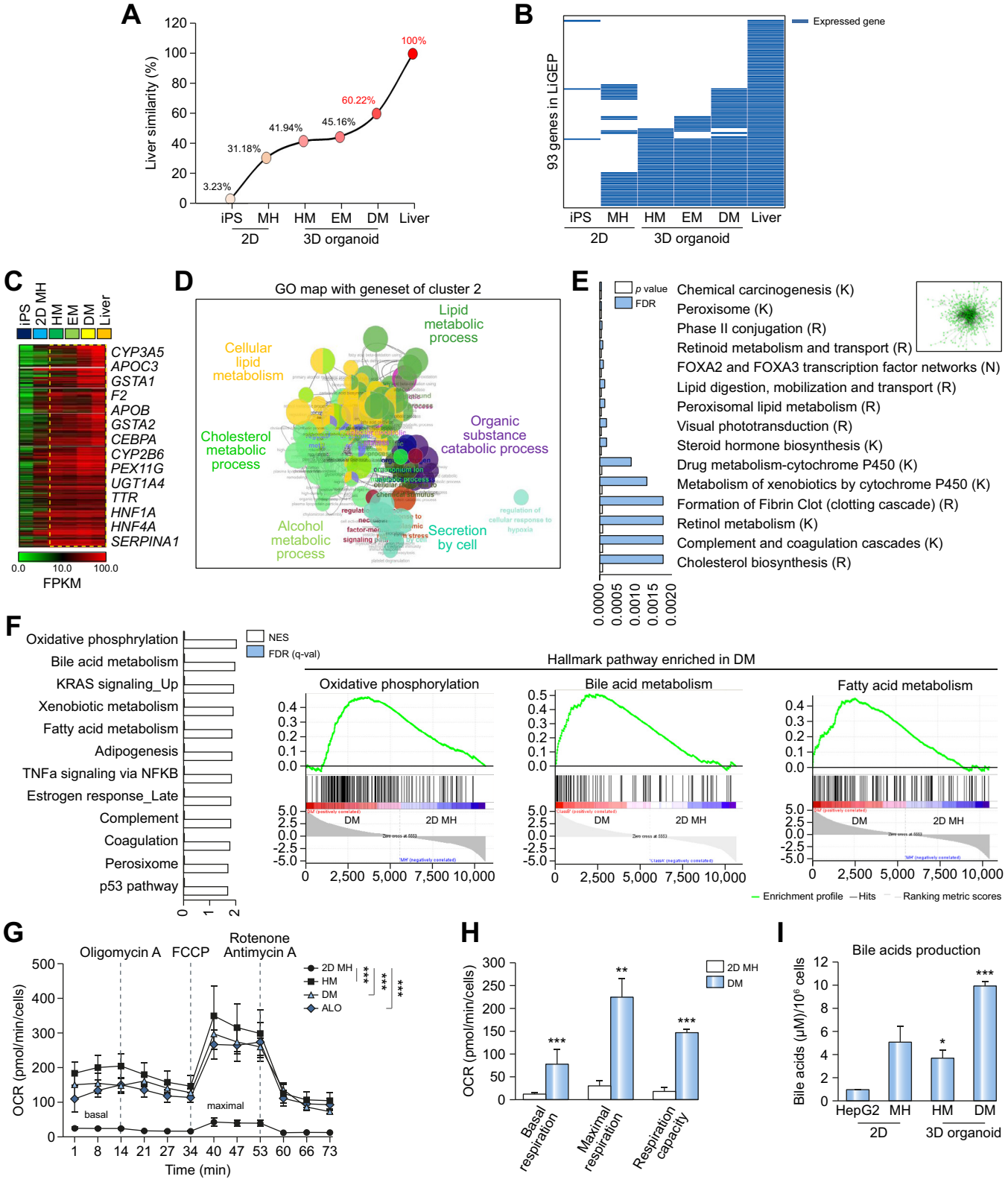

(Fig. 6F). Most importantly, real-time monitoring of mitochondrial toxicity based on the OCR precisely indicated the impairment of mitochondrial respiration by trovafloxacin at a low dose of treatment, such as 0.8 μM (Fig. 6G) and 4 μM (Fig. 6H), while almost no toxicity was detected at these concentrations for levofloxacin, and a mild inhibitory effect was exhibited only with the 100 μM treatment (Fig. S16D). Therefore, these data indicate that human hepatocyte-like liver organoids retain their native drug-metabolizing activity and susceptibility to toxicity and thus could be used as a potential model to evaluate drug toxicity.

Regenerative and inflammatory response in human hepatic organoids

Next, we analyzed the recovery potential and inflammatory response of our organoids after treatment with high-dose APAP (Fig. 7A) because a change in regenerative capacity is one of the main characteristics of liver damage. After 5 days of 20 mM APAP treatment, organoids presented severe morphological damage (Fig. 7B), though they recovered well by day 7 when the medium was changed on day 4.5, after 60 h of APAP treatment (Fig. 7A). In time-lapse imaging, an organoid badly damaged by APAP treatment, as shown by the black small sphere, recovered remarkably well after the change of medium (Video S2). Damaged organoids recovered well in terms of organoid size (Fig. 7C) and the cell cycle (Fig. S17A), and from apoptosis (Fig. 7B) after the change of medium. Although niche cells, including immune cells, are not present in our organoid system, simple epithelial responses, such as damage-associated molecular patterns, which have been reported to induce inflammation and then contribute to regeneration or pathological injury,[40] were found, and an increase of ROS production upon APAP treatment was detected (Fig. 7D and Fig. S17B). The decreased expression and cytosolic translocation of high-mobility group box 1 protein (HMGB1) and diminished expression of Ki67, E-cadherin, and mitochondria marker Tom20 were observed in organoids after 5 days or 60 h of 20 mM APAP, although expression levels recovered close to the control level after APAP was removed (Fig. 7D). The expression of the autophagy marker LC3B was more strongly induced by 60 h of APAP treatment than by 5 days of the treatment, which presented a similar pattern as the ATP contents (Fig. 7E) and GSH/GSSG ratio (Fig. 7F). Long-term damage conditions may prevent autophagy-dependent recovery. Consistently, expression of pro-inflammatory mediators *IL-1β*, *IL-6*, and *IL-8* and pathological mediators *TNFα* and *FasL* were strongly induced in the APAP-treated organoids, although the expression of an anti-inflammatory mediator *IL-10* was remarkably enhanced on day 5 of the recovery condition (Fig. 7G). These results demonstrate that our human hepatocyte-like liver organoids could be a useful model for understanding regenerative and simple inflammatory responses after hepatotoxic injury.

Human hepatic organoids for modeling steatosis pathology and drug screening

Finally, we developed a steatosis model through excess treatment with oleate and palmitate, the most abundant fatty acid (FA) found in the human liver,[30] to recapitulate the liver pathology (Fig. 8) because gene sets for FA metabolism, including FA uptake (*FABP1*, *ACSL5*, and *CD36*), hydrolysis (*MGLL*), and β-oxidation (*ACADVL*, *HADHB*, and *ETFDH*), were enriched in the transcriptome profiles of organoids (Fig. 5D-F, Fig. 8A, Fig. S6e, Fig. S11B, and Fig. S12A), and metabolites involved in lipid metabolism were distinctly increased in the organoid (Fig. S5k). Treatment with 0.8 mM oleate for 3 days increased the intracellular lipid accumulation compared with that after treatment with the bovine serum albumin (BSA) control; however, the combination treatment with 0.5 mM oleate and 0.25 mM palmitate more potently induced lipid accumulation, as evidenced by a dark morphology (Fig. S18A). Under the DM condition, increased Oil red O and Nile red stained lipid droplets were observed in the untreated- or BSA treated-control compared to the HM controls (Fig. S18B). The gene expression level differences of *FASN*, *FABP1*, *PLIN2*, and *SREBP* were a 9.07-, 7.16-, 4.86-, and 1.98-fold increase in the HM condition, but a 1.33-, 1.89-, 2.98-, and 1.31-fold increase in the DM condition compared with BSA, respectively (Fig. S18C). Thus, we performed steatosis modeling in the HM condition (Fig. 8) because responses upon FA treatment were clearly more distinguishable in the HM than the DM condition, and HM does not require at least 6 days of additional maturation with DM. In this condition, glucose uptake (Fig. S19A) and consumption (Fig. S19B) and glycogen contents (Fig. S19C) were decreased by the FA treatment, while the expression of gluconeogenesis involving genes (Fig. S19D) and glucose synthesis stimulated by glucagon (Fig. S19E) were increased in the FA-treated organoids. However, inflammatory responses were not induced in our simple steatosis model without immune cells (Fig. S19F and I), although the ATP contents (Fig. S19G) and GSH/GSSG ratio (Fig. S19H) were slightly decreased by the FA treatment while inflammatory signaling, including cytokines and chemokines, was strongly increased by lipopolysaccharide (LPS) or carbon tetrachloride (CCl_4) treatment (Fig. S19I). The steatosis induction was aggravated by additional treatment with etomoxir, an irreversible inhibitor of carnitine palmitoyltransferase-1 (CPT1), by blocking the carnitine shuttle that transports FAs to the mitochondrial membrane for β-oxidation.[30] Thus, the FA +etomoxir treatment promoted darkening of the organoids (Fig. S20A) and significant accumulation of intracellular lipid droplets observed by bright field microscopy and Nile red

Fig. 5. Transcriptome profiles and functional assessment of human hepatic organoids. (A) Liver similarity by the LiGEP algorithm and (B) Expressed genes of LiGEP of iPSCs; 2D MHs; HM-, EM-, and DM-cultured organoids; and human liver tissue. (C) Heat map of cluster 2 differentially expressed genes in human hepatic organoids from Fig. S11A. Representative genes are shown on the right. (D) Gene ontology map for the cluster 2 genes. (E) Functional pathways enriched in the cluster 2 genes. (F) List of gene sets enriched in DM compared with 2D MHs. Enrichment plot of the top-ranked subset signatures of hallmarks in DM; oxidative phosphorylation, bile acid metabolism, and fatty acid metabolism. (G) OCR was measured by an XFe96 Flux Analyzer in the 2D MH, HM- and DM-cultured organoids, and adult liver tissue-derived hepatic organoids ALOs. Data are the mean ± SEM (n = 5) and analyzed by Student's *t* test. An ATP synthase inhibitor (1.5 μM oligomycin, ETC complex V inhibitor), uncoupler (1 μM FCCP), and complex I inhibitor (0.5 μM rotenone) + complex III inhibitor (0.5 μM antimycin A) were sequentially added at each indicated time point. (H) Basal and maximal OCR and respiration capacity of 2D MHs and DM-cultured organoids. Data are the mean ± SEM (n = 5) and analyzed by Student's *t* test. (I) Quantitation of bile acid production in the 2D MHs and HM- and DM-cultured organoids. 2D cultured HepG2 cells were used as a control. Data are the mean ± SEM (n = 3) and analyzed by Student's *t* test. $^{*}p$ <0.05; $^{**}p$ <0.01; and $^{***}p$ <0.001. 2D MHs, 2D differentiated mature hepatocytes; ALOs, adult liver tissue-derived hepatic organoids; DM, differentiation medium; EM, expansion medium; HM, hepatic medium; iPSC, induced pluripotent stem cells; LiGEP, liver-specific gene expression panel; OCR, oxygen consumption rate.

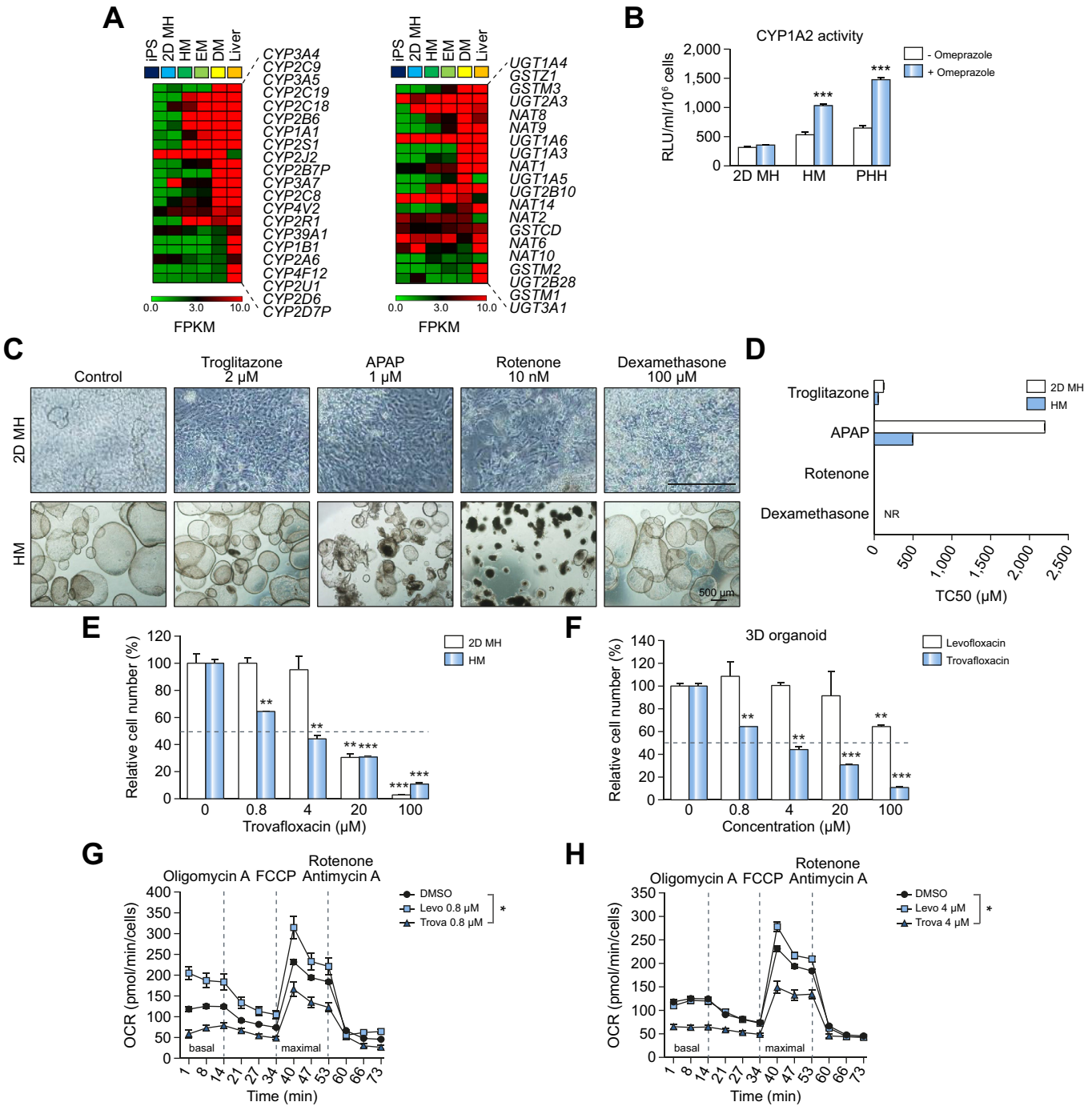

Fig. 6. Toxicological outcome prediction using human hepatic organoids. (A) Heat map of genes involved in phase I drug-metabolizing CYP enzymes (left) and phase II detoxification enzymes (right) in human hepatic organoids. (B) CYP1A2 enzyme activity in the 2D MHs, HM-cultured organoids, and PHHs with or without 150 μM omeprazole treatment for 48 h. Data are the mean ± SEM (n = 3) and analyzed by Student's *t* test. (C) Representative morphology of each indicated drug-treated 2D MHs (upper) and HM-cultured organoids (lower) at 6 days after treatment. (D) Toxic concentration (TC_{50}) was determined by cell numbers after 6 days of treatment with troglitazone (0.2–500 μM, human Cmax = 6.29 μM), APAP (16–10,000 μM, human Cmax = 165.4 μM), rotenone (10 nM-100 μM, human Cmax = not available), and dexamethasone (0.4–100 μM, human Cmax = NR, no response) in the 2D MHs and HM-cultured organoids. Data are the mean ± SEM (n = 3). (E) Relative toxicity is represented by cell numbers under treatment for 6 days with the indicated concentrations of trovafloxacin in the 2D MHs and HM-cultured organoids. Data are the mean ± SEM (n = 3) and analyzed by Student's *t* test. (F) Relative toxicity is represented by cell numbers under treatment for 6 days with the indicated concentrations of levofloxacin and trovafloxacin in the HM-cultured organoids. Data are the mean ± SEM (n = 3) and analyzed by Student's *t* test. (G and H) OCR was measured by an XFe96 Flux Analyzer in the HM-cultured organoids treated with DMSO, 0.8 μM (G) and 4 μM (H) levofloxacin or trovafloxacin for 6 days. An ATP synthase inhibitor (3 μM oligomycin, ETC complex V inhibitor), uncoupler (3 μM FCCP), and complex I inhibitor (1.5 μM rotenone) + complex III inhibitor (1.5 μM antimycin A) were sequentially added at each indicated time point. Data are the mean ± SEM (n = 5) and analyzed by Student's *t* test. $^{*}p$ <0.05; $^{**}p$ <0.01; and $^{***}p$ <0.001. 2D MHs, 2D differentiated mature hepatocytes; APAP, acetaminophen; DM, differentiation medium; EM, expansion medium; HM, hepatic medium; OCR, oxygen consumption rate; PHHs, primary human hepatocytes.

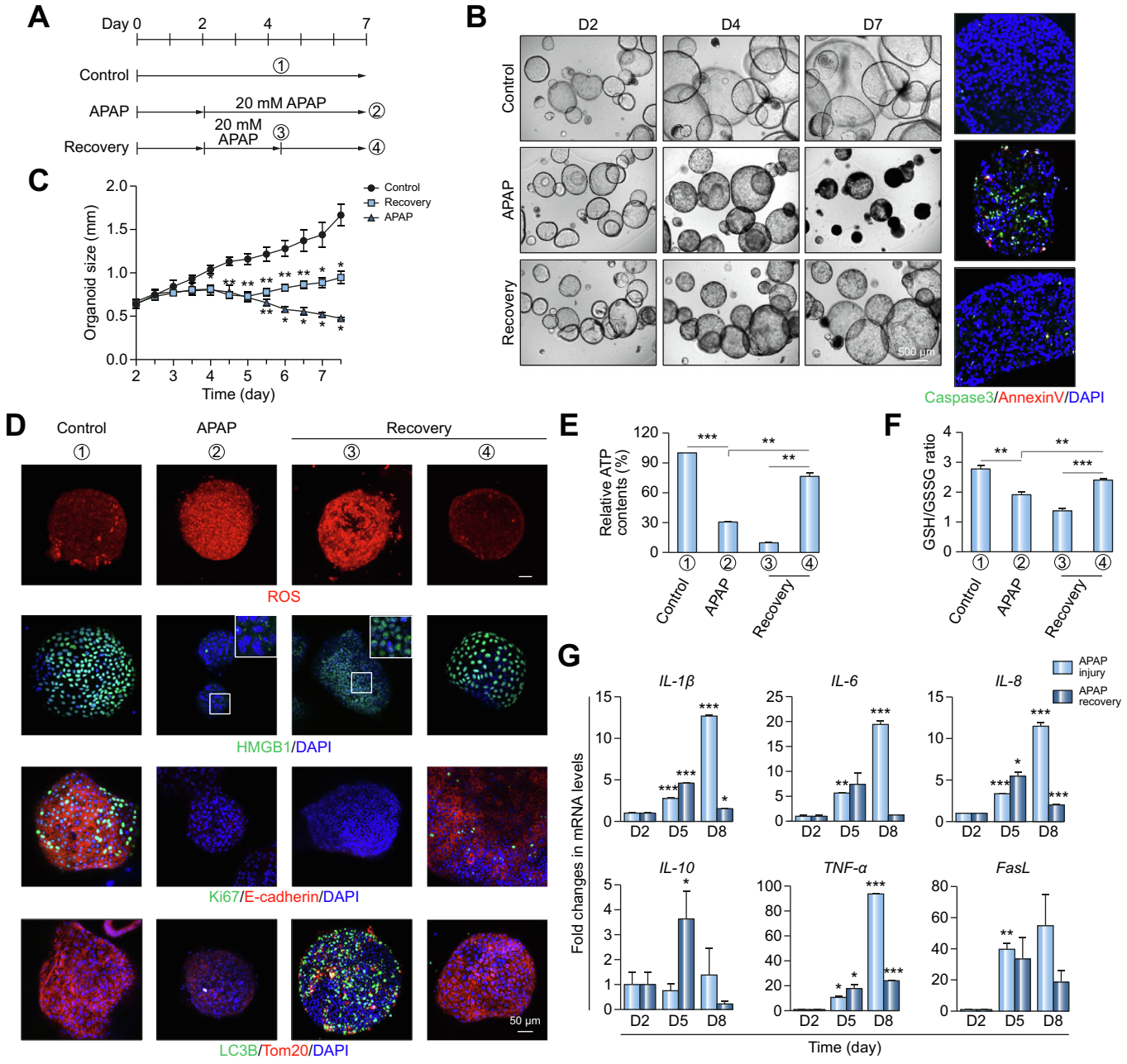

Fig. 7. Recovery and inflammatory response after APAP treatment in human hepatic organoids. (A) Time frame of APAP injury and recovery. (B) Representative organoid morphology of the control, APAP injury, and recovery condition on day 2, 4, and 7. Caspase3- and annexin V-stained apoptotic cells in the organoids on day 7 are shown in the right panel. (C) The organoid sizes were compared every 12 h after APAP treatment in each group. Data are the mean ± SEM (n = 20) and analyzed by Student's *t* test. (D) Representative fluorescence images of organoids stained with dihydroethidium for ROS detection and immunofluorescence images of organoids stained with each indicated antibody. An enlarged image of cytosolic translocation of HMGB1 (white box) is shown in the upper right of the second line. (E) ATP contents and (F) GSH/GSSG ratio were determined in each indicated condition. Data are the mean ± SEM (n = 3) and analyzed by Student's *t* test. (G) mRNA expression level of inflammatory response-related genes in APAP injured- and recovered-organoids on each indicated day. Data are the mean ± SEM (n = 3) and analyzed by Student's *t* test. **p* <0.05; ***p* <0.01; and ****p* <0.001. APAP, acetaminophen; ROS, reactive oxygen species.

staining (Fig. 8B). The intracellular triglyceride concentration was indeed strongly increased by the FA+etomoxir treatment compared with that in either the BSA control or FA treatment alone (Fig. 8C), and functionally, the mitochondrial respiration as determined by the OCR was extensively decreased by the FA+etomoxir treatment (Fig. 8D). Conversely, the steatosis induction was greatly ameliorated by treatment with L-carnitine by promoting mitochondrial carnitine shuttle. The FA +L-carnitine treatment obviously improved the phenotype of the organoids (Fig. S20A), and the lipid accumulation was potently decreased by the FA+L-carnitine treatment compared with the FA treatment alone (Fig. 8B and C). Furthermore, the mitochondrial OCR was clearly recovered by the FA+L-carnitine treatment, while the FA-treated organoids presented a functionally impaired OCR (Fig. 8D). In addition, we applied an antidiabetic drug, metformin, based on its function in decreasing hepatic steatosis.[41,42] The FA+metformin treatment slightly recovered the morphology (Fig. S20A) and lipid

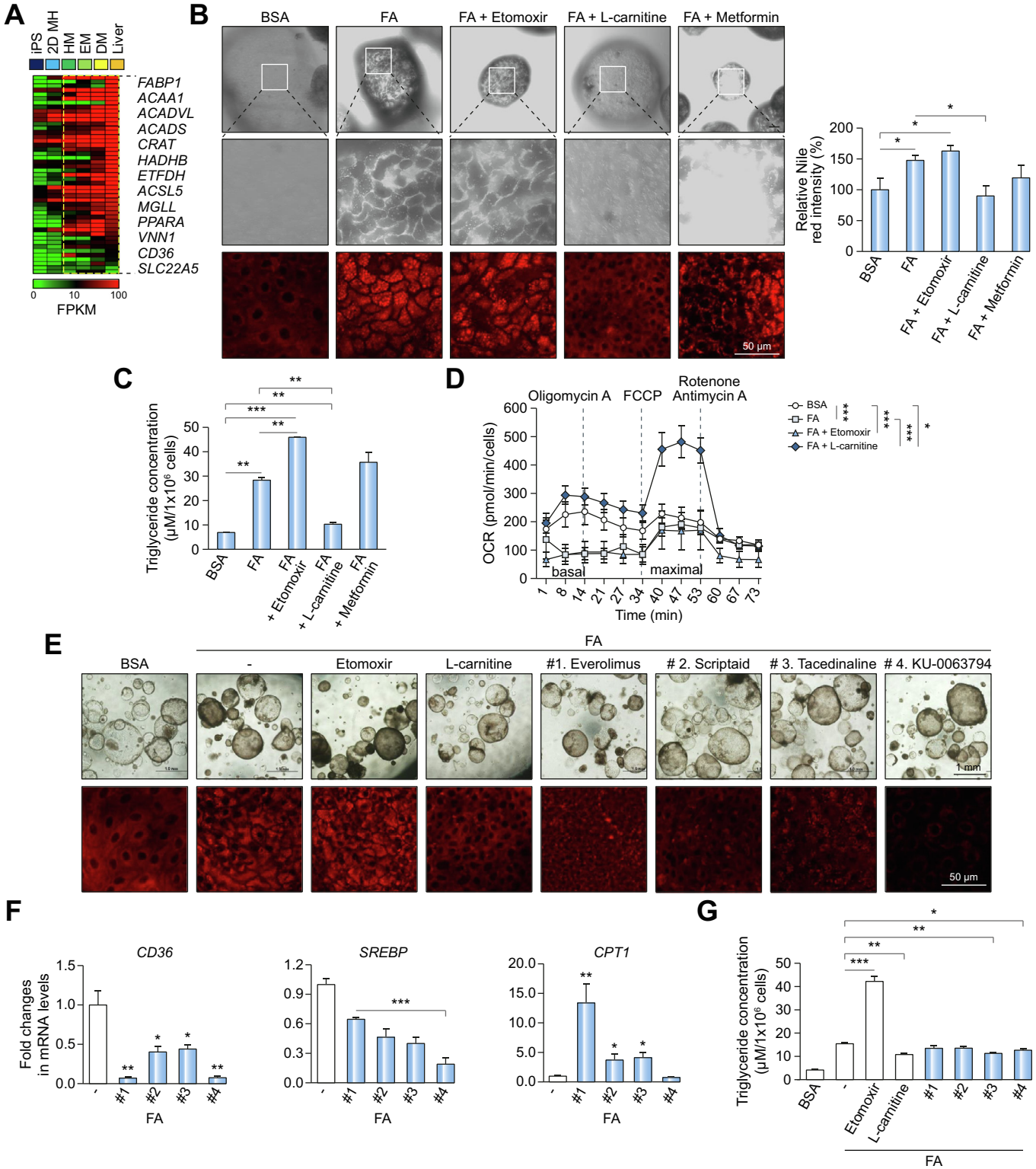

Fig. 8. Human hepatic organoids for modeling steatosis pathology and drug screening. (A) Heat map of the genes involved in FA metabolism in human hepatic organoids. (B) Representative morphology of BSA-, FA (oleate and palmitate), and FA+etomoxir (CPT1 inhibitor)-, FA+L-carnitine-, and FA+metformin-treated HM-cultured organoids on day 3 (upper panel). An enlarged image of lipid droplets (white box) is shown in the middle panel. Representative confocal fluorescence images of each indicated organoid stained with Nile red (lower panel). The relative Nile red intensity is shown in the right panel. Data are the mean ± SEM (n = 3) and analyzed by Student's *t* test. (C) Quantitation of the triglyceride concentration in each indicated organoid per million cells on day 3. Data are the mean ± SEM (n = 3) and analyzed by Student's *t* test. (D) OCR was measured by an XFe96 Flux Analyzer in each indicated organoid on day 3. Data are the mean ± SEM (n = 5) and analyzed by Student's *t* test. (E) Representative morphology of each indicated organoid on day 3 after treatment with autophagy library compounds (upper panel). Confocal images of each indicated organoid stained with Nile red (lower panel). The top hit compounds from an autophagy library are presented as #1–4. (F) mRNA expression levels of each specific gene in the organoids treated with the selected top hits on day 3. Data are the mean ± SEM (n = 3) and analyzed by Student's *t* test. (G) Quantitation of the triglyceride concentration in each indicated organoid per million cells on day 3. Data are the mean ± SEM (n = 3) and analyzed by Student's *t* test. $^{*}p$ <0.05; $^{**}p$ <0.01; and $^{***}p$ <0.001. BSA, bovine serum albumin; FA, fatty acid; HM, hepatic medium.

accumulation, as assessed by staining with Nile red (Fig. 8B and Fig. S20B) and Oil red O (Fig. S20B), although it had little effect on the decrease in triglycerides (Fig. 8C) under our conditions. Finally, we applied the organoids for anti-steatosis drug screening based on a high-content analysis of Nile red staining (Fig. 8E) because our organoid model responded well to steatosis pathologic conditions and Nile red staining evidently indicated FA accumulation (Fig. 8B). The top 4 compounds recovering the phenotype and lipid accumulation were identified in a library of autophagy, which could target hepatic steatosis (Fig. 8E).[43] Notably, the anti-steatotic effects of the top 2 compounds were conferred by the inhibition of lipogenesis and the increase of lipid oxidation.[44,45] In accordance with the phenotype, the expression of genes, such as hepatic fatty acid translocase *CD36*, the *de novo* lipogenesis related factors *SREBP* and *PPAR-γ*, the related enzyme *FASN*, and a lipid droplet protein *PLIN2*, was potently downregulated after treatment with the top hit compounds (Fig. 8F and Fig. S20C). The expression of genes related to β-oxidation *CPT1*, *SLC25A20*, *ETFB*, and *PPAR-α* was upregulated after treatment with the compounds (Fig. 8F and Fig. S20C). The triglyceride concentration was indeed decreased by the top hit compounds (Fig. 8G). Overall, in our attempt to validate the system, the organoids preserved mature liver functionality with respect to detoxification and pathologic responses, and their expandability confer the potential for use as a toxicity prediction and drug-validation platform.

Discussion

The development of physiologically and pathologically relevant hepatic models that preserve functional human liver characteristics over the long-term *in vitro* has remained a challenge. Herein, we provide a method of generating expandable and functionally mature human PSC-derived hepatocyte-like liver organoids. Our protocol is highly efficient and reproducible and takes a relatively short time (approximately 22 days) after starting differentiation. The established organoids were scalable and showed i) self-renewal, ii) rapid proliferation and maturation, and iii) long-term storage and good viability after cryopreservation. Furthermore, the organoids were functionally beneficial in i) protein and lipid metabolism, ii) active mitochondrial bioenergetics, iii) regenerative and inflammatory responses, iv) drug metabolism and detoxification, and v) the recapitulation of liver pathology over 20 passages. Thus, these organoids may be a stable and robust *in vitro* hepatic model that can facilitate an understanding of liver development and regeneration, providing insights for metabolic studies and disease modeling, as well as toxicity assessment and drug screening for personalized medicine.

In this study, we define for the first time a novel culture condition in which PSC-derived hepatic organoids have functions comparable to those of tissue-derived liver organoids. PSC-derived organoids exhibit self-renewal while maintaining their mature hepatic characteristics over long-term culture in "HM", which is a novel composition we newly define here, and "EM and DM" are the exactly same as reported by Clevers' group.[22] We excluded R-spondin and FGF10 in "HM", which were included in EM, because they are dispensable to the growth of organoids and costly. However, R-spondin, a Wnt agonist, and FGF10, which functions in the patterning of the primitive gut,[46] may be the critical components for overcoming the differentiation barrier. Since we could not find abundant expression of *ALB* and *CYP3A4* without EM before the DM treatment, it may be essential to perform further hepatic differentiation by promoting the survival/proliferation of hepatoblasts/hepatocytes. Compared with DM, the boost in proliferation by forskolin[22] and bFGF[47] for hepatic progenitors and by nicotinamide and ITS for hepatocytes[48] and the boost in hepatic maturation by OSM[49] may be the critical stimuli derived from "HM". Wnt and FGF signaling derived by cardiac mesoderm is essential for inducing ventral foregut endoderm and subsequently producing hepatic progenitors in liver development.[47,49] Forskolin, a cAMP inducer, increases the expression of *LGR5*,[22] a receptor for R-spondin and a liver stem cell marker that potentiates Wnt signaling.[50] bFGF mediates specification of hepatic progenitors[47] by substituting for cardiac mesodermal signals.[51] Therefore, "HM" could simultaneously intensify the self-renewal and hepatic maturation potential of organoids, thereby providing useful conditions for long-term *in vitro* experimentation.

To validate the feasibility of our organoids, we intensively analyzed their molecular foundations and functional competences. First, we demonstrated the quantitative similarity of our organoids to human liver tissue using LiGEP.[36] Given that hepatocytes, the major parenchymal cells, constitute approximately 80% of liver tissue, a similarity of 60.22% in the DM-cultured organoids would be a meaningful level achievable by an *in vitro* differentiation system. hPSC-derived organoids have been reported to have a less mature phenotype *in vitro*;[52–54] however, our model shows at least an advantage of rapid kinetics of the generation/differentiation of organoids, an absolute amount of albumin production, and potent mitochondrial respiration compared with those of adult liver tissue-derived organoids. Second, a detailed transcriptome analysis revealed mature characteristics of the organoids, with enriched gene sets such as those for drug-metabolizing enzymes, mitochondrial and peroxisomal lipid metabolism, and coagulation cascades. Importantly, the liver, which is a key metabolic organ, is highly reliant on energy-generating mitochondrial functions.[55] OXPHOS was a top-enriched pathway in differentiated hepatic organoids compared with conventional 2D differentiated hepatocytes. Indeed, the bioenergetic profile revealed that the respiration capacity and ATP production rate were apparently higher in the organoids than in the 2D culture. An analysis of the metabolites and metabolism-related gene expression also revealed metabolic reprogramming of iPSCs from glycolysis to mitochondrial OXPHOS during organoid generation.

Furthermore, other prominent pathways enriched in the organoids included gene sets involved in bile acid and lipid metabolism, which is also crucial in liver function.[55] Gene expression related to bile acid synthesis and the expression levels of the bile acid receptor and transporter were enhanced in the organoids, and bile acid production and polarized epithelial cells with a bile canaliculi-like structure were strongly detected in differentiated organoids. Gene expression related to lipid metabolism, including FA uptake and metabolism, triglyceride hydrolysis, β-oxidation, and cholesterol metabolism and secretion, was also clearly enhanced in the organoids. Fatty acyl CoA was indeed distinctly increased in the organoids. In addition, the organoids responded well to excess FA treatment and reflected steatosis phenotypes such as lipid droplet accumulation, increased triglycerides, and mitochondrial impairment.

Notably, our organoids readily produced a disease model (such as hepatic steatosis) that comprised a relatively uniform

size and homogenous phenotype. Furthermore, genetic disease modeling using organoids derived from patient iPSCs or whole-genome-scale genetically engineered PSCs is comparatively simple because of the clonal properties of PSCs.[56] Therefore, this robust and convenient organoid model may be applicable as a drug-screening system and, in this study, it provided reliable drug targets in a small-scale setting. However, our current model has limitations when it comes to recapitulating further progression of severe liver damage because of the absence of the adipose tissue and gut, outside the liver, as well as of niche cells from within the liver, such as Kupffer cells, hepatic stellate cells, and sinusoidal endothelial cells, which are important for triggering inflammation and fibrosis.[40] Indeed, the inflammatory responses were not induced in our simple steatosis model, which is in accordance with a report indicating that lipid accumulation is insufficient to induce inflammation in the liver,[57] although inflammatory signaling presented a sufficient response under APAP, LPS or CCl_4 treatment, and steatosis-induced organoids revealed impaired glucose metabolism. Thus, a niche-enriched- and/or multi-organoid platform will help to recapitulate the actual inflammatory pathologies.

Most importantly, upon chronic exposure to hepatotoxic drugs, the organoids in HM exhibited significantly higher sensitivity than the 2D differentiated monolayers of hepatocytes at clinically relevant concentrations. In the case of trovafloxacin, which was withdrawn from the market due to severe hepatotoxicity, the TC_{50} in the organoids was 2.7 μM, which is below the human plasma Cmax concentration (4.1 μM), while the TC_{50} in 2D MHs was 141 μM. Technically, the real-time monitoring of hepatotoxicity based on the high-content analysis of ROS, GSH, and nuclear structures, as well as cellular bioenergetics as determined by the mitochondrial OCR, could potentially predict the toxicological responses at concentrations close to the therapeutic exposure levels. Thus, our method using iPSC-based patient-specific organoids would enable the high-throughput and early prediction of drug-induced liver injury (DILI) by parent drugs or their reactive metabolites with increased sensitivity. However, for the application to further high-quality large-scale drug testing, DM conditions with high levels of activity of drug-metabolizing enzymes could provide a better platform, which may reflect more mature and accurate liver functionality. In addition, the organoids may be applicable to prediction models for hepatocellular toxicity, cholestatic toxicity by hepatobiliary inhibiting drugs, and the mixed-type toxicity of DILI, because the organoids contain both hepatocytes and cholangiocytes with a polarized bile canaliculi-like structure. Furthermore, modeling drug-induced steatosis[55] as well as diet/metabolism-induced steatosis may be possible. In addition, the mechanical compliance of 3D cultures may be associated with the superiority of the organoids because we previously found that soft niches close to that of native liver tissue enhanced the functionality of a 3D liver model.[58] Functional improvements following epigenetic changes are a possible explanation, although further detailed mechanistic studies on the functional maturation of our organoids are needed.

Recently, human hepatic organoids derived from PSCs were reported,[56] and although the method of generation was different from ours, similar compositions of the 2 main types of cells (hepatocytes and cholangiocytes) were generated without other cellular complexity. Those organoids mainly provided an application for the genetic disease model of bile duct formation with genome editing. Our organoids are morphologically indistinguishable from and as functionally competent as adult tissue-derived liver organoids. Here, we analyzed detailed properties of our organoids and demonstrated the potential of the organoids as a screening platform for toxicity prediction and drug evaluation. Based on the final application and prior optimization, HM-cultured organoids and DM-cultured organoids could be used selectively, depending on the specific properties required. Further studies are required to determine additional applications of complex organ-like structures with cellular complexity, and to determine the utility of *in vivo* transplantation for regenerative medicine.

Financial support

This work was supported by the KRIBB Initiative of the Korea Research Council of Fundamental Science and Technology; the National Research Foundation (NRF) grant funded by the Korean government (MSIT) (NRF-2019R1A2C2004992); the Korea Health Technology R&D Project through the KHIDI, funded by the Ministry of Health & Welfare (HI16C0312); and the Bio & Medical Technology Development Program of the NRF & funded by the Korean government (MSIT) (NRF-2018M3A9H3023077).

Conflict of interest

The authors declare no conflicts of interest that pertain to this work.

Please refer to the accompanying ICMJE disclosure forms for further details.

Authors' contributions

Study conception and design: Mun SJ, Ryu J, Son YS, Son M, Kim J, Jung C, Chung K, and Son MJ. Acquisition of data: Mun SJ, Ryu J, Oh SJ, Kim D, Kim SJ, Yoo HJ, and Son MJ. Analysis and interpretation of data: Mun SJ, Ryu J, Lee M, Oh SJ, Cho H, Kim D, Kim SJ, Yoo HJ, Lee H, Chung K, and Son MJ. Drafting of manuscript: Lee H, Chung K, and Son MJ. Critical revision: Mun SJ, Ryu J, Lee M, Oh SJ, Lee H, Chung K, and Son MJ

Acknowledgments

We thank the DMPK core facility and the Metabolomics core at the ConveRgence mEDIcine research cenTer (CREDIT), Asan Medical Center for support and instrumentation.

Supplementary data

Supplementary data to this article can be found online at https://doi.org/10.1016/j.jhep.2019.06.030.

References

Author names in bold designate shared co-first authorship

[1] Nguyen DG, Funk J, Robbins JB, Crogan-Grundy C, Presnell SC, Singer T, et al. Bioprinted 3D primary liver tissues allow assessment of organ-level response to clinical drug induced toxicity in vitro. PLoS One 2016;11:e0158674.

[2] Levy G, Bomze D, Heinz S, Ramachandran SD, Noerenberg A, Cohen M, et al. Long-term culture and expansion of primary human hepatocytes. Nat Biotechnol 2015;33:1264–1271.

[3] Heidariyan Z, Ghanian MH, Ashjari M, Farzaneh Z, Najarasl M, Rezaei Larijani M, et al. Efficient and cost-effective generation of hepatocyte-like

cells through microparticle-mediated delivery of growth factors in a 3D culture of human pluripotent stem cells. Biomaterials 2018;159:174–188.
[4] Ma X, Qu X, Zhu W, Li YS, Yuan S, Zhang H, et al. Deterministically patterned biomimetic human iPSC-derived hepatic model via rapid 3D bioprinting. Proc Natl Acad Sci U S A 2016;113:2206–2211.
[5] **Underhill GH**, **Khetani SR**. Bioengineered liver models for drug testing and cell differentiation studies. Cell Mol Gastroenterol Hepatol 2018;5:426–439 e421.
[6] **Bell CC**, **Hendriks DF**, Moro SM, Ellis E, Walsh J, Renblom A, et al. Characterization of primary human hepatocyte spheroids as a model system for drug-induced liver injury, liver function and disease. Sci Rep 2016;6:25187.
[7] Richert L, Baze A, Parmentier C, Gerets HHJ, Sison-Young R, Dorau M, et al. Cytotoxicity evaluation using cryopreserved primary human hepatocytes in various culture formats. Toxicol Lett 2016;258:207–215.
[8] **Zhang K**, **Zhang L**, Liu W, Ma X, Cen J, Sun Z, et al. In Vitro Expansion of Primary Human Hepatocytes with Efficient Liver Repopulation Capacity. Cell Stem Cell 2018;23:806-819 e804.
[9] **Kim Y**, **Kang K**, Lee SB, Seo D, Yoon S, Kim SJ, et al. Small molecule-mediated reprogramming of human hepatocytes into bipotent progenitor cells. J Hepatol 2019;70:97–107.
[10] **Si-Tayeb K**, **Noto FK**, Nagaoka M, Li J, Battle MA, Duris C, et al. Highly efficient generation of human hepatocyte-like cells from induced pluripotent stem cells. Hepatology 2010;51:297–305.
[11] **Coll M**, **Perea L**, Boon R, Leite SB, Vallverdu J, Mannaerts I, et al. Generation of hepatic stellate cells from human pluripotent stem cells enables in vitro modeling of liver fibrosis. Cell Stem Cell 2018;23:101–113 e107.
[12] Sampaziotis F, de Brito MC, Geti I, Bertero A, Hannan NR, Vallier L. Directed differentiation of human induced pluripotent stem cells into functional cholangiocyte-like cells. Nat Protoc 2017;12:814–827.
[13] Sampaziotis F, de Brito MC, Madrigal P, Bertero A, Saeb-Parsy K, Soares FAC, et al. Cholangiocytes derived from human induced pluripotent stem cells for disease modeling and drug validation. Nat Biotechnol 2015;33:845–852.
[14] **Wang Y**, **Qin J**, **Wang S**, **Zhang W**, Duan J, Zhang J, et al. Conversion of human gastric epithelial cells to multipotent endodermal progenitors using defined small molecules. Cell Stem Cell 2016;19:449–461.
[15] Zhao D, Chen S, Cai J, Guo Y, Song Z, Che J, et al. Derivation and characterization of hepatic progenitor cells from human embryonic stem cells. PLoS One 2009;4:e6468.
[16] **Yu B**, **He ZY**, You P, Han QW, Xiang D, Chen F, et al. Reprogramming fibroblasts into bipotential hepatic stem cells by defined factors. Cell Stem Cell 2013;13:328–340.
[17] **Panciera T**, **Azzolin L**, **Fujimura A**, Di Biagio D, Frasson C, Bresolin S, et al. Induction of expandable tissue-specific stem/progenitor cells through transient expression of YAP/TAZ. Cell Stem Cell 2016;19:725–737.
[18] **Huang P**, **Zhang L**, **Gao Y**, **He Z**, Yao D, Wu Z, et al. Direct reprogramming of human fibroblasts to functional and expandable hepatocytes. Cell Stem Cell 2014;14:370–384.
[19] Zhu S, Rezvani M, Harbell J, Mattis AN, Wolfe AR, Benet LZ, et al. Mouse liver repopulation with hepatocytes generated from human fibroblasts. Nature 2014;508:93–97.
[20] **Vyas D**, **Baptista PM**, Brovold M, Moran E, Gaston B, Booth C, et al. Self-assembled liver organoids recapitulate hepatobiliary organogenesis in vitro. Hepatology 2017.
[21] **Broutier L**, **Andersson-Rolf A**, **Hindley CJ**, Boj SF, Clevers H, Koo BK, et al. Culture and establishment of self-renewing human and mouse adult liver and pancreas 3D organoids and their genetic manipulation. Nat Protoc 2016;11:1724–1743.
[22] **Huch M**, **Gehart H**, **van Boxtel R**, Hamer K, Blokzijl F, Verstegen MM, et al. Long-term culture of genome-stable bipotent stem cells from adult human liver. Cell 2015;160:299–312.
[23] Sampaziotis F, Justin AW, Tysoe OC, Sawiak S, Godfrey EM, Upponi SS, et al. Reconstruction of the mouse extrahepatic biliary tree using primary human extrahepatic cholangiocyte organoids. Nat Med 2017;23:954–963.
[24] Takebe T, Sekine K, Kimura M, Yoshizawa E, Ayano S, Koido M, et al. Massive and reproducible production of liver buds entirely from human pluripotent stem cells. Cell Rep 2017;21:2661–2670.
[25] Takebe T, Sekine K, Enomura M, Koike H, Kimura M, Ogaeri T, et al. Vascularized and functional human liver from an iPSC-derived organ bud transplant. Nature 2013;499:481–484.
[26] Takebe T, Zhang RR, Koike H, Kimura M, Yoshizawa E, Enomura M, et al. Generation of a vascularized and functional human liver from an iPSC-derived organ bud transplant. Nat Protoc 2014;9:396–409.
[27] Takebe T, Enomura M, Yoshizawa E, Kimura M, Koike H, Ueno Y, et al. Vascularized and complex organ buds from diverse tissues via mesenchymal cell-driven condensation. Cell Stem Cell 2015;16:556–565.
[28] Camp JG, Sekine K, Gerber T, Loeffler-Wirth H, Binder H, Gac M, et al. Multilineage communication regulates human liver bud development from pluripotency. Nature 2017;546:533–538.
[29] Siller R, Naumovska E, Mathapati S, Lycke M, Greenhough S, Sullivan GJ. Development of a rapid screen for the endodermal differentiation potential of human pluripotent stem cell lines. Sci Rep 2016;6:37178.
[30] Kruitwagen HS, Oosterhoff LA, Vernooij I, Schrall IM, van Wolferen ME, Bannink F, et al. Long-term adult feline liver organoid cultures for disease modeling of hepatic steatosis. Stem Cell Reports 2017;8:822–830.
[31] Gripon P, Rumin S, Urban S, Le Seyec J, Glaise D, Cannie I, et al. Infection of a human hepatoma cell line by hepatitis B virus. Proc Natl Acad Sci U S A 2002;99:15655–15660.
[32] Andersson TB, Kanebratt KP, Kenna JG. The HepaRG cell line: a unique in vitro tool for understanding drug metabolism and toxicology in human. Expert Opin Drug Metab Toxicol 2012;8:909–920.
[33] Ho CM, Dhawan A, Hughes RD, Lehec SC, Puppi J, Philippeos C, et al. Use of indocyanine green for functional assessment of human hepatocytes for transplantation. Asian J Surg 2012;35:9–15.
[34] Komori M, Nishio K, Ohi H, Kitada M, Kamataki T. Molecular cloning and sequence analysis of cDNA containing the entire coding region for human fetal liver cytochrome P-450. J Biochem 1989;105:161–163.
[35] Gieseck 3rd RL, Hannan NR, Bort R, Hanley NA, Drake RA, Cameron GW, et al. Maturation of induced pluripotent stem cell derived hepatocytes by 3D-culture. PLoS One 2014;9:e86372.
[36] **Kim DS**, **Ryu JW**, **Son MY**, Oh JH, Chung KS, Lee S, et al. A liver-specific gene expression panel predicts the differentiation status of in vitro hepatocyte models. Hepatology 2017;66:1662–1674.
[37] Kostadinova R, Boess F, Applegate D, Suter L, Weiser T, Singer T, et al. A long-term three dimensional liver co-culture system for improved prediction of clinically relevant drug-induced hepatotoxicity. Toxicol Appl Pharmacol 2013;268:1–16.
[38] Lazarczyk DA, Goldstein NS, Gordon SC. Trovafloxacin hepatotoxicity. Dig Dis Sci 2001;46:925–926.
[39] Watkins PB. Insight into hepatotoxicity: the troglitazone experience. Hepatology 2005;41:229–230.
[40] Schuster S, Cabrera D, Arrese M, Feldstein AE. Triggering and resolution of inflammation in NASH. Nat Rev Gastroenterol Hepatol 2018;15:349–364.
[41] Rouabhia S, Milic N, Abenavoli L. Metformin in the treatment of non-alcoholic fatty liver disease: safety, efficacy and mechanism. Expert Rev Gastroenterol Hepatol 2014;8:343–349.
[42] Woo SL, Xu H, Li H, Zhao Y, Hu X, Zhao J, et al. Metformin ameliorates hepatic steatosis and inflammation without altering adipose phenotype in diet-induced obesity. PLoS One 2014;9:e91111.
[43] Mao Y, Yu F, Wang J, Guo C, Fan X. Autophagy: a new target for nonalcoholic fatty liver disease therapy. Hepat Med 2016;8:27–37.
[44] Love S, Mudasir MA, Bhardwaj SC, Singh G, Tasduq SA. Long-term administration of tacrolimus and everolimus prevents high cholesterol-high fructose-induced steatosis in C57BL/6J mice by inhibiting de-novo lipogenesis. Oncotarget 2017;8:113403–113417.
[45] **Gaur V**, **Connor T**, Sanigorski A, Martin SD, Bruce CR, Henstridge DC, et al. Disruption of the class IIa HDAC corepressor complex increases energy expenditure and lipid oxidation. Cell Rep 2016;16:2802–2810.
[46] Touboul T, Hannan NR, Corbineau S, Martinez A, Martinet C, Branchereau S, et al. Generation of functional hepatocytes from human embryonic stem cells under chemically defined conditions that recapitulate liver development. Hepatology 2010;51:1754–1765.
[47] Twaroski K, Mallanna SK, Jing R, DiFurio F, Urick A, Duncan SA. FGF2 mediates hepatic progenitor cell formation during human pluripotent stem cell differentiation by inducing the WNT antagonist NKD1. Genes Dev 2015;29:2463–2474.
[48] Prasajak P, Leeanansaksiri W. Developing a new two-step protocol to generate functional hepatocytes from Wharton's jelly-derived mesenchymal stem cells under hypoxic condition. Stem Cells Int 2013;2013:762196.
[49] Gordillo M, Evans T, Gouon-Evans V. Orchestrating liver development. Development 2015;142:2094–2108.

[50] Ruffner H, Sprunger J, Charlat O, Leighton-Davies J, Grosshans B, Salathe A, et al. R-Spondin potentiates Wnt/beta-catenin signaling through orphan receptors LGR4 and LGR5. PLoS One 2012;7:e40976.
[51] Jung J, Zheng M, Goldfarb M, Zaret KS. Initiation of mammalian liver development from endoderm by fibroblast growth factors. Science 1999;284:1998–2003.
[52] **Zachos NC**, **Kovbasnjuk O**, Foulke-Abel J, In J, Blutt SE, de Jonge HR, et al. Human enteroids/colonoids and intestinal organoids functionally recapitulate normal intestinal physiology and pathophysiology. J Biol Chem 2016;291:3759–3766.
[53] Dedhia PH, Bertaux-Skeirik N, Zavros Y, Spence JR. Organoid models of human gastrointestinal development and disease. Gastroenterology 2016;150:1098–1112.
[54] Xinaris C, Brizi V, Remuzzi G. Organoid models and applications in biomedical research. Nephron 2015;130:191–199.
[55] Begriche K, Massart J, Robin MA, Borgne-Sanchez A, Fromenty B. Drug-induced toxicity on mitochondria and lipid metabolism: mechanistic diversity and deleterious consequences for the liver. J Hepatol 2011;54:773–794.
[56] Guan Y, Xu D, Garfin PM, Ehmer U, Hurwitz M, Enns G, et al. Human hepatic organoids for the analysis of human genetic diseases. JCI Insight 2017;2.
[57] **Monetti M**, **Levin MC**, Watt MJ, Sajan MP, Marmor S, Hubbard BK, et al. Dissociation of hepatic steatosis and insulin resistance in mice overexpressing DGAT in the liver. Cell Metab 2007;6:69–78.
[58] **Lee HJ**, **Son MJ**, Ahn J, Oh SJ, Lee M, Kim A, et al. Elasticity-based development of functionally enhanced multicellular 3D liver encapsulated in hybrid hydrogel. Acta Biomater 2017;64:67–79.